

# Temperature-insensitive sensor for glucose brix measurement based on compact spindle-shaped structure with two-mode fiber\*

DONG Miaoyun, TONG Zhengrong\*\*, ZHANG Weihua, LI Peng, WU Meng, and TIAN Xue

*Engineering Research Center of Optoelectronic Devices and Communication Technology, Ministry of Education, Tianjin Key Laboratory of Film Electronic and Communication Devices, School of Integrated Circuit Science and Engineering, Tianjin University of Technology, Tianjin 300384, China*

(Received 18 June 2022; Revised 25 August 2022)

©Tianjin University of Technology 2022

A temperature-insensitive sensor for glucose brix measurement based on compact spindle-shaped structure with two-mode fiber (TMF) is proposed. Due to the bending of optical fiber caused by flame baking, some of the light energy transmitted in the core leaks into the cladding area as an evanescent wave, which excites the higher-order cladding mode of the sensor. The experimental results show that when the length of TMF is 3 cm and the bending diameter is 4 mm, the maximum glucose brix sensitivity of the sensor is 0.368 nm/% from 0 to 21%. The sensor is insensitive to temperature from 10 °C to 50 °C, which can avoid the problem of temperature cross-sensitivity. A compact spindle-shaped sensor is a potential effective sensor with a simple structure, easy fabrication and low cost. The sensor can be used to detect glucose content in areas such as crops quality assessment and the research of pharmacy and bioengineering.

**Document code:** A **Article ID:** 1673-1905(2022)12-0737-6

**DOI** <https://doi.org/10.1007/s11801-022-2106-6>

Until now, optical Mach-Zehnder interferometer (MZI) sensors have been widely used to measure a variety of physical parameters<sup>[1]</sup>, including temperature<sup>[2]</sup>, refractive index (RI)<sup>[3]</sup>, humidity<sup>[4]</sup>, micro-displacement<sup>[5]</sup> and fluid level<sup>[6]</sup>. The sensors have a compact size, light weight, low cost, and good resistance to electromagnetic interference, which make them applicable in harsh environments. Recently, many researchers have explored various bent fiber structures, such as balloon-like<sup>[7]</sup>, ring-shaped<sup>[8]</sup>, S-shaped<sup>[9]</sup> and U-shaped<sup>[10]</sup> structures, for the measurement of various physical parameters. These structures only need to bend the fiber without damaging the external surface of the optical fiber<sup>[11-13]</sup>. In addition, bending of the fiber makes some light energy in the core of fiber leak into the cladding for transmission, resulting in a powerful optical fiber attenuation in the bent area. And optical fiber fade field is sensitive to external RI changes.

Measuring glucose brix is a method for assessing the ripeness and quality of fruits and vegetables, and it has great applications and future prospects in the pharmacy and bioengineering. Therefore, sensor research related to the measurement of glucose brix is becoming more and more important. For example, LOKMAN et al<sup>[14]</sup> studied

a dumbbell-shaped structure inline MZI for the detection of glucose, the sensitivity of the sensor is 0.04 nm/% in the range of 0—12%. JIANG et al<sup>[15]</sup> presented a label-free biosensor based on graphene oxide (GO) and glucose oxidase (GOD) functionalized tilted fiber grating (TFG) with large tilted angle for low concentration glucose detection, and the sensitivity of the sensor is ~0.24 nm/mM in the range of 0—8 mM. WANG et al<sup>[16]</sup> proposed a biconical sensor based on a cascade structure of three-core optical fibers, with a glucose sensitivity of 195.67 pm/% for glucose concentrations range from 1% to 15%.

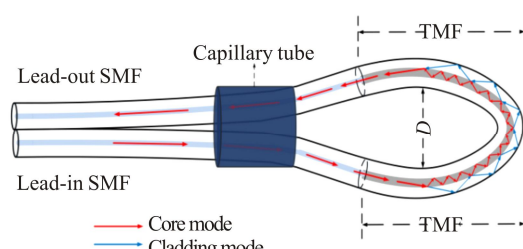
In this paper, we present a temperature-insensitive sensor for glucose brix measurement based on a compact spindle-shaped structure with two-mode fiber (TMF). The simulation experiments of TMF with different lengths and bending diameters are given, and it is concluded that the results are better when the length of TMF is 3 cm and the bending diameter is 4 mm. The experimental results show that the glucose brix highest sensitivity is 0.368 nm/% from 0 to 21%. The sensor is insensitive to temperature in the range of 10—50 °C, which can avoid the problem of temperature cross-sensitivity.

Fig.1 is a schematic of the proposed sensor. The short

\* This work has been supported by the National Natural Science Foundation of China (No.62003237), the Tianjin Enterprise Technology Commissioner Project (No.20YDTPJC01700), the State Key Laboratory of Applied Optics (No.SKLA02020001A02), and the Tianjin Municipal Education Commission Scientific Research Project (No.2017ZD15).

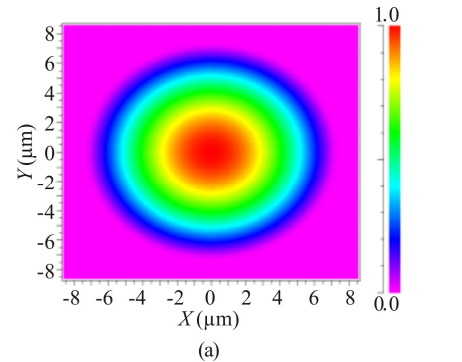
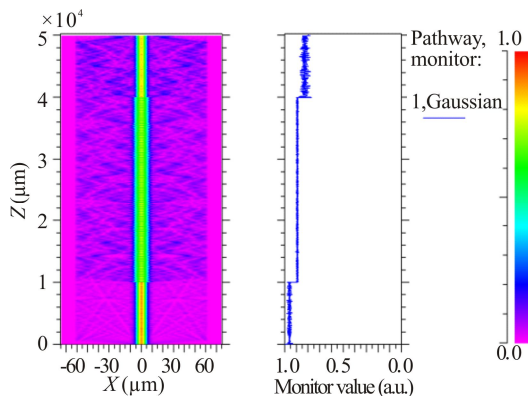
\*\* E-mail: [tjtongzhenrong@163.com](mailto:tjtongzhenrong@163.com)

axis  $D$  is defined as the bending diameter of the sensor, and  $L$  is defined as the length of the TMF. In the manufacturing process, both ends of the TMF ( $14\ \mu\text{m}/125\ \mu\text{m}$ ) after peeling off the coating layer are connected with a single mode fiber (SMF) ( $8.2\ \mu\text{m}/125\ \mu\text{m}$ ), respectively. Then a lead-in SMF and a lead-out SMF are penetrated into the same end of a capillary tube (inner diameter  $500\ \mu\text{m}$ ). At the top of the capillary tube, the SMF-TMF-SMF (STS) structure is extruded into a balloon-like structure. When the center of the balloon-like structure with STS structure is suspended in the flame of the candle, due to heating by flame, the balloon-like structure will rapidly shrink inward in less than 1 s to form a spindle-shaped structure with a diameter greater than 1 cm. Then a spindle-shaped structure with a diameter greater than 1 cm will be suspended at a distance of  $\sim 1\ \text{mm}$  around the outer flame of the candle to bake it for  $\sim 2\ \text{s}$  to form the proposed spindle-shaped structure. During the experiment, the flame should remain stable. As shown in Fig.1, the light enters the spindle-shaped structure from the lead-in SMF. Most of the light continues to travel along the fiber core. Due to the bending of the optical fiber, some of the light in the core leaks into the outer cladding of the TMF, which excites the high-order cladding mode of the TMF. When they reach the curved end, some light is coupled back to the lead-out SMF, resulting in multimode interference.

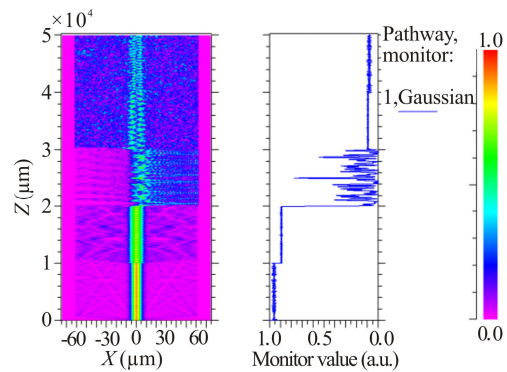


**Fig.1 Proposed sensor structure**

Different sizes of SMF-TMF-SMF structures are simulated by using Rsoft software as shown in Fig.2 and Fig.3. The background refractive index is 1, the central wavelength is  $1\ 550\ \text{nm}$ , and both the lead-in SMF and lead-out SMF are 1 cm in length.



(a)



(b)

**Fig.2 Simulated optical field distributions and the transverse mode profiles of the sensor when TMF length is 3 cm: (a) Straight fiber; (b) Bent fiber with bending diameter of 4 mm**

Fig.2(a) and (b) show the comparison of the transverse mode field distributions between straight fiber and simulated bent optical fiber. From the comparison results, it can be found that some energy of the core in the bent TMF leaks into the cladding of the optical fiber, resulting in mode leakage and transmission loss. As shown in Fig.2(a), when the TMF is not bent, the light energy travels along the fiber core in a straight line with little interference. As shown in Fig.2(b), when the lead-in light energy is transmitted in the bent fiber, the mode energy coupling will occur to some extent because the bending makes some of the light transmitted in the core leak into the cladding area as an evanescent wave. Then most of the light after bending is coupled back to the lead-out SMF. Based on the mode field analysis, simulated interference spectra are added, as shown in Fig.3. Fig.3(a)

shows the simulated interference spectra of straight fibers and different bending diameters when TMF is 3 cm. Fig.3(b) shows the simulated interference spectra of TMF with different lengths and bending diameter of 4 mm. It can be seen that the number of dips and extinction ratio are related to the bending diameter and the length of TMF.

When an optical fiber is bent, the RI distribution in the optical fiber changes as shown in Fig.4 because of the elastic-optic effect.

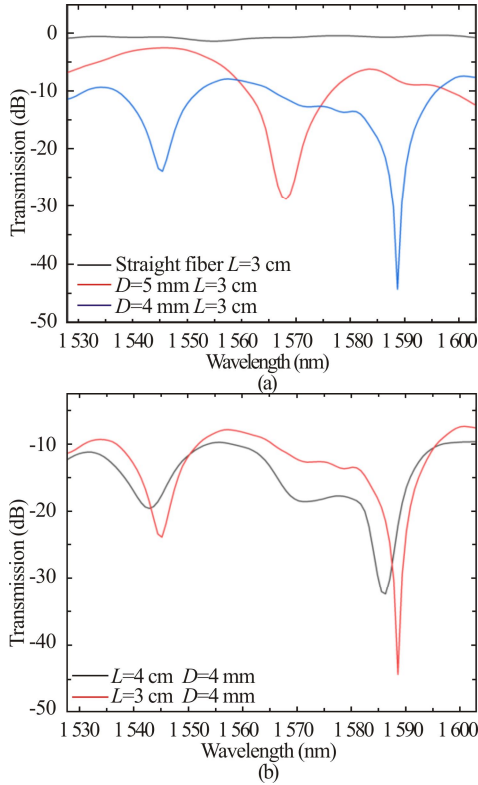


**Fig.3 Simulated interference spectra of (a) straight fiber and bent fiber with different bending diameters, and (b) bent fiber with different lengths of TMF**

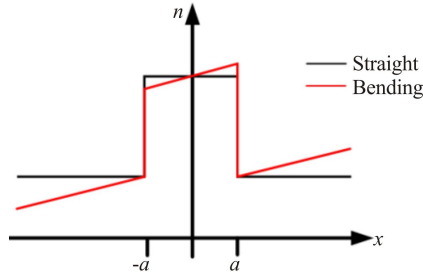


**Fig.4 RI distribution of the straight/bent TMF**

Compared with the straight fiber, the internal RI of bent TMF is reduced and the external RI is increased. By using the equivalent refractive index model<sup>[17]</sup>, the RI distribution after the conformal mapping is as follows

$$n(x) = n_0 \left(1 + \frac{x}{R_{\text{eff}}}\right), \quad (1)$$

where  $n(x)$  and  $n_0$  are the RI distributions as the TMF is bent and straight, respectively.  $x$  is perpendicular to the

bent TMF axis. The equivalent bending radius  $R_{\text{eff}}$  can be expressed as<sup>[17]</sup>

$$R_{\text{eff}} = \frac{R}{1 - n_0^2 / 2[P_{12} - \nu(P_{11} + P_{12})]}, \quad (2)$$

where  $R=D/2$  is the bending radius of the TMF.  $P_{11}$  and  $P_{12}$  are components of the photoelastic tensor.  $\nu$  is the Poisson ratio.

The design principle of this sensor is similar to in-line MZI, and the core mode and the cladding mode are transmitted together in the fiber causing interference. Therefore, the total light intensity  $I$  can be equivalent to

$$I = I_{\text{core}} + \sum_{m=1}^i I_{\text{clad}}^m + 2 \sum_{m=1}^i \sqrt{I_{\text{core}} I_{\text{clad}}^m} \cos \Delta\varphi_{\text{core-clad}}, \quad (3)$$

where  $I_{\text{core}}$  is the intensity of the core mode in TMF, and  $I_{\text{clad}}^m$  is the intensity of the  $m$ -order cladding mode. The phase difference  $\Delta\varphi_{\text{core-clad}}$  can be expressed as

$$\Delta\varphi_{\text{core-clad}} = \frac{2\pi\Delta n_{\text{eff}}}{\lambda} L_{\text{eff}}, \quad (4)$$

where  $\lambda$  and  $L_{\text{eff}}$  are the wavelength of the incident light and the effective sensing length of the bending area, respectively. The length of the long half-axis of the spindle-shaped structure is about twice that of the short half-axis  $R$  by many practical measurements, so the effective simulated bending length  $L_{\text{eff}}$  is defined as  $L_{\text{eff}} \approx \pi R + 2R$ .  $\Delta n_{\text{eff}}$  is the difference between the effective RI of the core mode  $n_{\text{eff}}^{\text{core}}$  and the cladding modes  $n_{\text{eff}}^{\text{clad}}$ . When the phase difference is satisfied with  $\Delta\varphi_{\text{core-clad}} = (2k + 1)\pi$  and  $k=0, 1, 2, 3, \dots$ , the transmission spectra in Eq.(4) reach the minimum. The interference dips occur. The resonant wavelength  $\lambda_{\text{dip}}$  can be presented as

$$\lambda_{\text{dip}} = \frac{2L_{\text{eff}}}{2k + 1} \Delta n_{\text{eff}}. \quad (5)$$

From Eq.(5), it can be deduced that the drift of interference dip can be expressed as

$$\Delta\lambda_{\text{dip}} = \frac{2\Delta n_c L_{\text{eff}}}{2k + 1} = \left(\frac{\Delta n_c}{\Delta n_{\text{eff}}}\right) \lambda_{\text{dip}}, \quad (6)$$

where  $\Delta n_c$  is the variation of  $\Delta n_{\text{eff}}$ . Therefore, the ambient physical parameters can be detected by monitoring the variation of the resonance wavelength  $\Delta\lambda_{\text{dip}}$ .

The relationship between the variation of brix of a glucose solution  $\Delta C_b$  and its the variation of the refractive index  $\Delta RI$  is as follows<sup>[18]</sup>

$$\Delta RI = \eta \Delta C_b, \quad (7)$$

where  $\eta$  is a constant. The glucose brix sensing characteristic formula can be written as

$$K_c = \frac{\Delta\lambda_{\text{dip}}}{\Delta C_b} = \frac{\Delta n_c}{\Delta n_{\text{eff}}} \cdot \frac{\lambda_{\text{dip}}}{\eta \Delta C_b}. \quad (8)$$

Because of the thermal-optical effect and thermal expansion effect of the optical fiber, changes in the ambient temperature around the sensor cause changes in the refractive index of optical materials, which results in the wavelength shift of the transmission spectrum. The temperature sensing characteristic formula can be expressed

as follows

$$K_T = \frac{\Delta\lambda_{\text{dip}}}{\Delta T} = \lambda_{\text{dip}}(\alpha + \Delta n_c), \quad (9)$$

where  $\alpha$  is the thermal expansion coefficient. Because the sensor is baked at high temperature in the flame, the thermal expansion effect of the material caused by the change of the external temperature has little effect on the mode of transmission. When the temperature changes from 10 °C to 50 °C,  $\Delta n_c$  is nearly zero. Therefore, the sensor is insensitive to temperature.

As shown in Fig.5, the main experimental devices used include a broadband source (BBS) in the spectral range of 1 528—1 603 nm, an optical spectrum analyzer (OSA), a thermometer, a solution beaker, an electric hot plate and a concentration meter in this experiment. Three samples are chosen for experimental comparison, namely Sensor-1 with the TMF length of 3 cm and bending diameter of 4 mm, Sensor-2 with the TMF length of 3 cm and bending diameter of 5 mm, Sensor-3 with the TMF length of 4 cm and bending diameter of 4 mm, respectively.

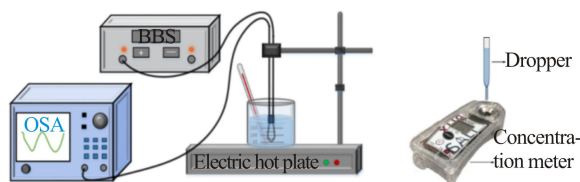
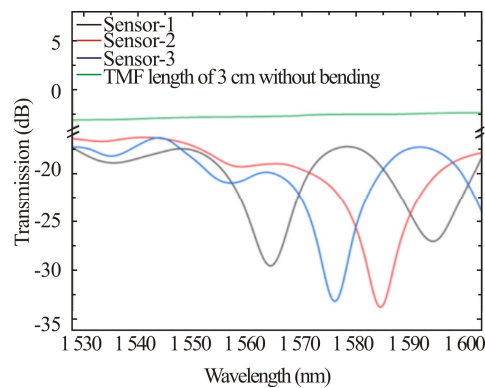


**Fig.5 Experimental setup of the glucose brix measurement**

Before experimental measurement, seven samples of glucose solutions with different brix are prepared using a concentration meter, ranging from 0 to 21 % of glucose brix. The different sample solutions configured are dripped into the glass container one by one and immersed in the sensor. After the sample solution is stabilized, the data in OSA are recorded, the measurements of each sample solution are repeated five times and the final result of each sample solution is the average of five measurements. After each sample solution is measured, the glassware and sensor are cleaned with clean water and dried to prevent residual glucose solutions from affecting the experimental measurements of the next set of solution samples. Fig.6 shows the interference spectra of the three sensors and those without bending sensor in a solution with 0 glucose brix. It is obvious that the sensor will not excite high-order cladding modes without bending.

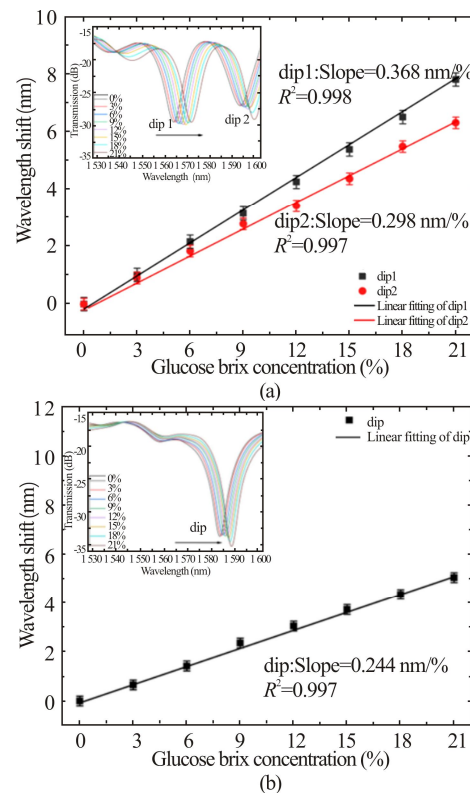
Fig.7 shows glucose brix contrast experiments for Sensor-1, Sensor-2 and Sensor-3, respectively. The dips of the sensor are significantly shifted when the glucose brix increases from 0 to 21%. As shown in Fig.7(a), with the increasing of glucose brix, the dips of the Sensor-1 are red-shifted, and the glucose brix sensitivity is 0.368 nm/% with a linear fitting of 0.998. As shown in Fig.7(b), the solution glucose brix rises and the dip of Sensor-2 shifts to a long wave, and the glucose brix sensitivity is 0.244 nm/% with a linear fitting of 0.997. As shown in Fig.7(c), the solution glucose brix rises and the

dips of the Sensor-3 shift to a long wave, and the glucose brix sensitivity is 0.301 nm/% with a linear fitting of 0.991. From the above comparative experimental results, when the TMF length is 3 cm and bending diameter is 4 mm, the glucose brix sensitivity is better. In order to solve the problem of temperature interference, further temperature experiments are carried out, and the method of water bath heating is used.



**Fig.6 Transmission spectra of sensors in solution without glucose brix**

From the results of the water bath temperature experiment in Fig.8, the sensors are insensitive to temperature in the temperature range of 10—50 °C, which effectively avoids the existence of temperature cross-sensitivity when measuring glucose brix, and the experimental results are consistent with the theoretical analysis. In addition, we need to further measure the stability of the Sensor-1 in the measurement of glucose brix as shown in Fig.9.



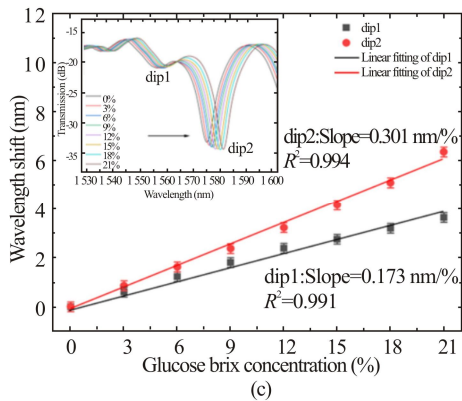


**Fig.7 Interference spectra and linear fitting diagrams at glucose brix concentrations of 0—21%: (a) Sensor-1; (b) Sensor-2; (c) Sensor-3**

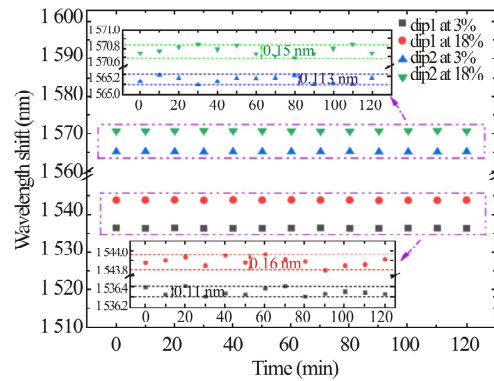


**Fig.9 Glucose brix measurement stability with the Sensor-1**

The proposed sensor is observed in 3% and 18% glucose brix, respectively. The ambient temperature remains constant. We need to observe and record data every 10 min. Fig.9 shows the results of the final stability measurements of Sensor-1, which indicates that the measured dip wavelength remains essentially unchanged for 120 min. When the glucose brix is 3%, the measurement variances of the dip1 and dip2 are 0.000 966 1 and 0.002 521, respectively. The maximum wavelength fluctuations of dip1 and dip2 are 0.11 nm and 0.113 nm, respectively. When the glucose brix is 18%, the measurement variances of the dip1 and dip2 are 0.003 944 and 0.002 068, respectively. The maximum wavelength fluctuations of dip1 and dip2 are 0.16 nm and 0.15 nm, respectively. The Sensor-1 has good measurement stability in the measurement of glucose brix. The fluctuations of interference dips are very little during 120 min. The fluctuations may be caused by random errors and reading errors.

In this paper, we study a novel MZI of compact spindle-shaped structure based on TMF for the measurement of glucose brix. When the length and bending diameter of TMF are 3 cm and 4 mm respectively, the experimental results show that the glucose brix sensitivity of the sensor is 0.368 nm/% in the range of 0—21% and the sensor is insensitive to temperature in the range of 10—50 °C, which can effectively avoid the existence of temperature cross-sensitivity when measuring glucose brix. The sensor has simple fabrication, low cost, good repeatability and stability, and has potential application prospects in crops quality assessment and the research of pharmacy and bioengineering.

**Statements and Declarations**

The authors declare that there are no conflicts of interest related to this article.

**References**

[1] LEI X Q, XU Y C, YU Y T, et al. Fiber in-line magnetic field sensor based on Mach-Zehnder interferometer

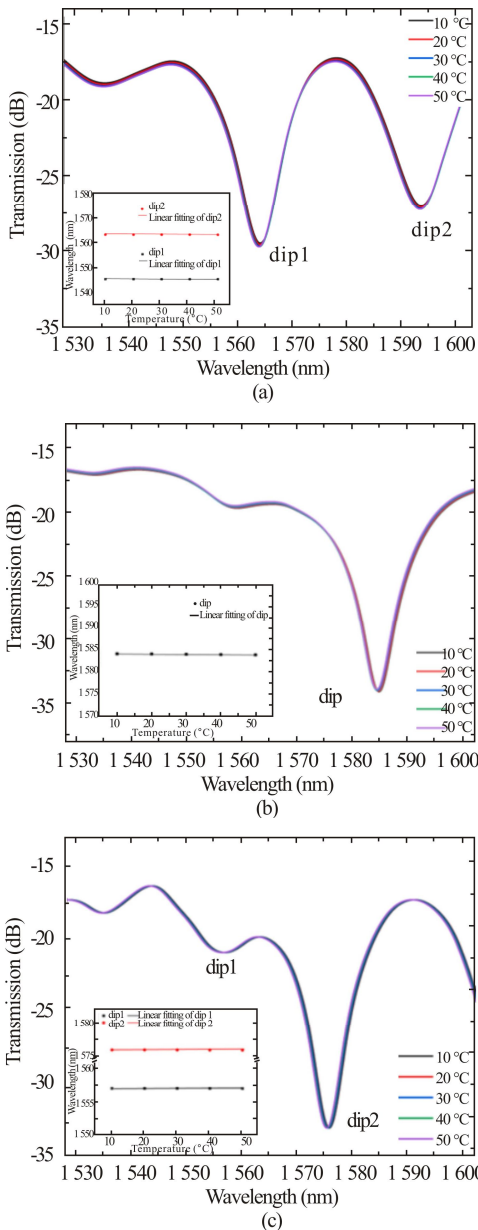


**Fig.8 Interference spectra and linear fitting diagrams in the range of 10—50 °C: (a) Sensor-1; (b) Sensor-2; (c) Sensor-3**

- integrated with magnetic fluid[J]. *Optoelectronics letters*, 2019, 15(1): 43-47.
- [2] JIANG Y, WANG T, LIU C, et al. Simultaneous measurement of refractive index and temperature with high sensitivity based on a multipath fiber Mach-Zehnder interferometer[J]. *Applied optics*, 2019, 58(15): 4085-4090.
- [3] LV R, LI J, HU H, et al. Miniature refractive index fiber sensor based on silica micro-tube and Au micro-sphere[J]. *Optical materials*, 2017, 72: 661-665.
- [4] JIA C G, JIA B, HUANG T, et al. High sensitivity relative humidity sensor based on SMTF structure coated with gelatin[J]. *Microwave and optical technology letters*, 2020, 62(11): 3432-3437.
- [5] WANG W, TAO C Y, GU Z D, et al. Sagnac fiber interferometer with the population grating for fiber Bragg grating dynamic strain sensing[J]. *Optoelectronics letters*, 2021, 17(12): 723-728.
- [6] LIU Y, LI Y, YAN X, et al. High refractive index liquid level measurement via coreless multimode fiber[J]. *IEEE photonics technology letters*, 2015, 27(20): 2111-2114.
- [7] LIU X, ZHAO Y, LV R Q, et al. High sensitivity balloon-like interferometer for refractive index and temperature measurement[J]. *IEEE photonics technology letters*, 2016, 28(13): 1485-1488.
- [8] ZHAO J, ZHAO Y, LV R Q, et al. Simultaneous measurement of temperature and pressure based on ring-shaped sensing structure with polymer coated no-core fiber[J]. *IEEE sensors journal*, 2021, 21(20): 22783-22791.
- [9] ZHANG X, PENG W. Fiber optic refractometer based on leaky-mode interference of bent fiber[J]. *IEEE photonics technology letters*, 2015, 27(1): 11-14.
- [10] DONG J, SANG M, WANG S, et al. Ultrasensitive label-free biosensor based on the graphene-oxide-coated-U-bent long-period fiber grating inscribed in a two-mode fiber[J]. *Journal of lightwave technology*, 2020, 39(12): 4013-4019.
- [11] TIAN K, FARRELL G, YANG W, et al. Simultaneous measurement of displacement and temperature based on a balloon-shaped bent SMF structure incorporating an LPG[J]. *Journal of lightwave technology*, 2018, 36(20): 4960-4966.
- [12] TIAN K, FARRELL G, WANG X, et al. Highly sensitive displacement sensor based on composite interference established within a balloon-shaped bent multimode fiber structure[J]. *Applied optics*, 2018, 57(32): 9662-9668.
- [13] LIU X, ZHAO Y, LV R Q, et al. Enhancement of RI sensitivity through bending a tapered-SMF-based balloon-like interferometer[J]. *Journal of lightwave technology*, 2016, 34(14): 3293-3299.
- [14] LOKMAN A, AROF H, HARUN S W. Dumbbell shaped inline Mach-Zehnder interferometer for glucose detection[J]. *Measurement*, 2015, 59: 167-170.
- [15] JIANG B Q, ZHANG K M, WANG C L, et al. Label-free glucose biosensor based on enzymatic graphene oxide-functionalized tilted fiber grating[J]. *Sensors and actuators B*, 2018, 254: 1033-1039.
- [16] WANG F, WANG R, WANG X, et al. Three-core fiber cascade asymmetric dual-taper robust structure for the simultaneous measurement of a mass concentration of a glucose solution and temperature[J]. *Optics communications*, 2020, 461: 125227.
- [17] SCHERMER R T, COLE J H. Improved bend loss formula verified for optical fiber by simulation and experiment[J]. *IEEE journal of quantum electronics*, 2007, 43(10): 899-909.
- [18] HARRIS J, LU P, XU Y, et al. Highly sensitive in-fiber interferometric refractometer with temperature and axial strain compensation[J]. *Optics express*, 2013, 21: 9996-10009.